Structural and kinetic insights into Pt/CNT catalysts during hydrogen generation from ammonia borane

Wenyao Chen [a,1], Zijun Wang [a,1], Xuezhi Duan [a,*], Gang Qian [a], De Chen [b], Xinggui Zhou [a]

[a] State Key Laboratory of Chemical Engineering, East China University of Science and Technology, 130 Meilong Road, Shanghai 200237, China
[b] Department of Chemical Engineering, Norwegian University of Science and Technology, N-7491 Trondheim, Norway

A B S T R A C T

Unraveling the structural and kinetic consequences of catalyst properties, which vary with the catalyst preparation methods, on their catalytic behaviors is of prime scientific and industrial importance. Exemplified by Pt/CNT-catalyzed hydrolytic dehydrogenation of ammonia borane (AB), this work examines the origin of the crucial impacts of the catalyst reduction methods (i.e., in situ reduction with AB and ex situ reduction with H_2) on the surface and electronic properties of the catalyst as well as the consequent hydrogen generation activity and durability. Kinetic and isotopic analyses reveal that the Pt/CNT-ex situ catalyst has low activation energy and a strong ability to activate water. The relationship between the catalyst structure and performance is established, and the unique surface (e.g., fewer Pt—O bonds) and electronic properties (e.g., higher Pt binding energy) of the Pt/CNT-ex situ catalyst are deemed to be responsible for the high activity and durability. The insights reported in this work highlight the importance of understanding the preparation-structure-performance relationship to guide the rational design of catalysts.

1. Introduction

Hydrogen, which is an ideal energy carrier due to its high energy efficiency and non-polluting nature, appears to be the best alternative for moving from traditional fossil fuels toward a sustainable energy future (Schlapbach and Zuttel, 2011; Dillon et al., 1997; Rosi et al., 2003; Sahiner et al., 2012). Ammonia borane (AB, NH_3BH_3) is considered one of the most promising chemical hydrogen storage materials because of its high hydrogen capacity of 19.6 wt%, good stability and non-toxicity (Staubitz et al., 2010; Demirci and Miele, 2009; Yadav and Xu, 2012; Peng and Chen, 2008; Marder, 2007; Sanyal et al., 2011; Tang et al., 2012). This

* Corresponding author.
E-mail address: xzduan@ecust.edu.cn (X. Duan).
[1] These authors contributed equally to this work.

material releases three equivalents of hydrogen in the presence of appropriate catalysts (e.g., Pt, Ru, Rh, Fe, Ni and Co) at mild reaction conditions via hydrolytic dehydrogenation (Chandra and Xu, 2006a, 2006b, 2007; Metin et al., 2009, 2010; Cao et al., 2013; Yao et al., 2014). On a commonly used and relatively high active Pt catalyst, the main reaction is $NH_3BH_3 + 4H_2O \rightarrow NH_4B(OH)_4 + 3H_2$ with $NH_3BH_2^* + H_2O^* \rightarrow NH_3BH_2OH^* + H^*$ as the rate-determining step (Chen et al., 2017). Recently, certain substantial efforts have been devoted to engineering of the catalyst microstructures and compositions toward more active sites (e.g., Pt(111)) and/or targeted Pt electronic properties for improved reactivity and/or durability (Chen et al., 2014a, 2014b, 2015; Wang et al., 2014; Cheng et al., 2007; Zhang et al., 2009).

For hydrolytic dehydrogenation of AB, a growing number of studies have been conducted to understand the crucial impacts of catalyst preparation methods on hydrogen generation activity (Mori et al., 2016; Yang et al., 2014; Wang et al., 2012, 2013; Akbayrak et al., 2016). Typically, amorphous non-noble (e.g., Fe, Co and Ni) nanocatalysts prepared by in situ reduction with $AB/NaBH_4$ showed much higher activity than those prepared by pre-reduction with $NaBH_4$ (Yan et al., 2008, 2009, 2010). This observation indicates the vital influences of AB on the catalyst

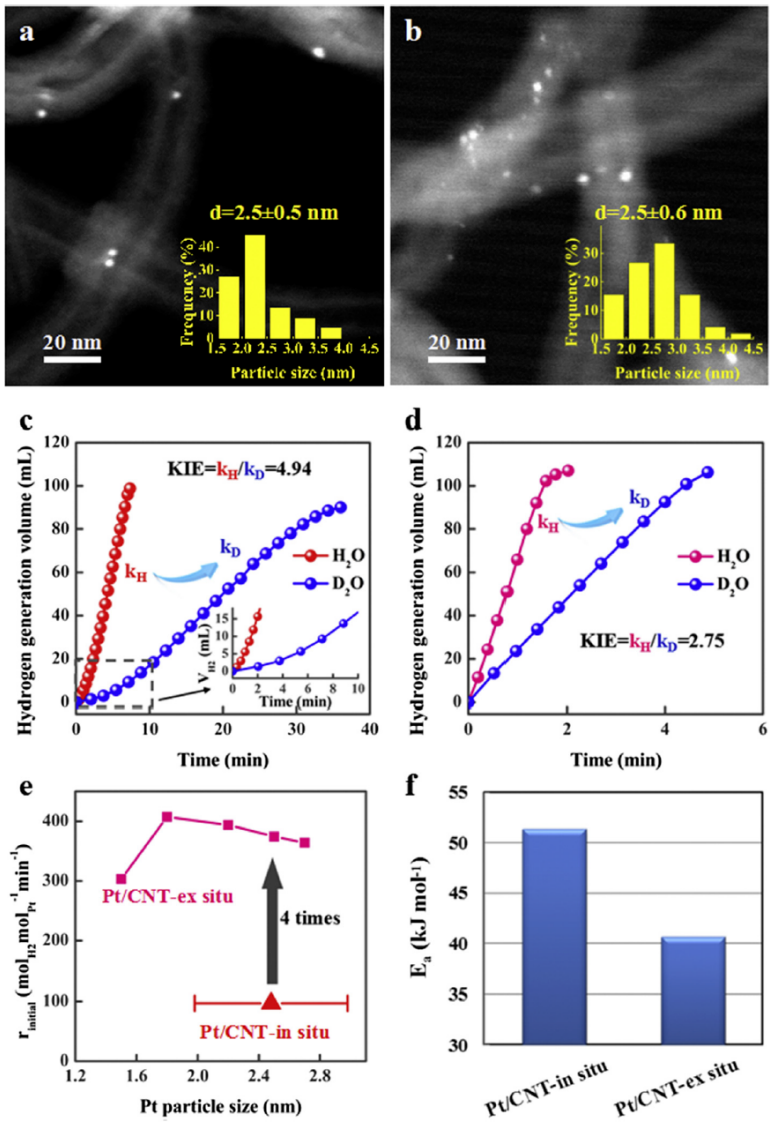

Fig. 1. Typical HAADF-STEM images and corresponding particle size distributions of Pt/CNT-in situ (a) and Pt/CNT-ex situ (b) catalysts. Hydrogen generation volume as a function of time over Pt/CNT-in situ (c) and Pt/CNT-ex situ (d) catalysts using H_2O or D_2O as the reactant at 30 °C. (e) Reaction rate as a function of Pt particle size over Pt/CNT-in situ and Pt/CNT-ex situ catalysts, where the reaction rate data of the Pt/CNT-ex situ catalysts with Pt particle sizes were obtained from Chen et al., 2014a. (f) Activation energies of the two catalysts.

properties. However, an open question still exists as to whether the in situ reduction with AB is also an effective method for synthesis of highly active noble catalysts (e.g., Pt). Additionally, certain unique reaction characteristics exist, e.g., the resultant B-containing product easily adsorbs on the catalyst surface and thereby affects the catalyst electronic properties (Chen et al., 2014a, 2015). Therefore, it is necessary to clarify the effects of catalyst reduction methods on the surface and electronic properties of the catalysts and correlate them with the hydrogen generation activity.

In addition to the crucial impacts of catalyst reduction methods on hydrogen generation activity, their impacts on durability are also an important issue. Our recent studies demonstrated that increasing the Pt binding energy of Pt/CNT catalysts gives rise to higher catalyst durability because of the suppressed adsorption of B-containing species on the catalyst surfaces (Chen et al., 2014a). In a consecutive effort, the variation of the surface and electronic properties of Pt/CNT catalysts with catalyst reduction methods was correlated with the durability.

The objectives of this study are to clarify the effects of catalyst reduction methods on the surface and electronic properties of Pt/CNT catalysts and thus the hydrogen generation activity and durability. Two types of Pt/CNT catalysts, i.e., Pt/CNT-in situ and Pt/CNT-ex situ, were prepared for reaction by two different reduction methods, i.e., in situ reduction with AB and ex situ reduction with H_2. The relationship between the catalyst structure and catalytic performance was established by combining kinetic and isotopic analyses with multiple techniques such as high resolution transmission electron microscopy (HRTEM), high angle annular dark field-scanning transmission electron microscopy (HAADF-STEM), X-ray photoelectron spectroscopy (XPS), inductively coupled plasma atomic emission spectrometry (ICP-AES) and Raman spectroscopy. To the best of our knowledge, this work offers the first evidence of a relationship among preparation (catalyst reduction), structure (Pt surface and electronic properties) and performance (hydrogen generation activity and durability) for Pt/CNT catalyzed hydrolytic dehydrogenation of AB.

2. Experimental

2.1. Catalyst preparation and testing

Pristine multi-walled carbon nanotubes (CNT, purchased from Beijing Cnano Technology Limited) with closed ends were used to immobilize the Pt precursor by incipient wetness impregnation. In detail, an aqueous solution of H_2PtCl_6 (Sinopharm Chemical Reagent Co. Ltd) was mixed with a certain amount of CNT, and the Pt loading based on the support was set to 1.5 wt%. The as-prepared sample was dried under stagnant air at room temperature for 12 h followed by drying at 80 °C for 12 h.

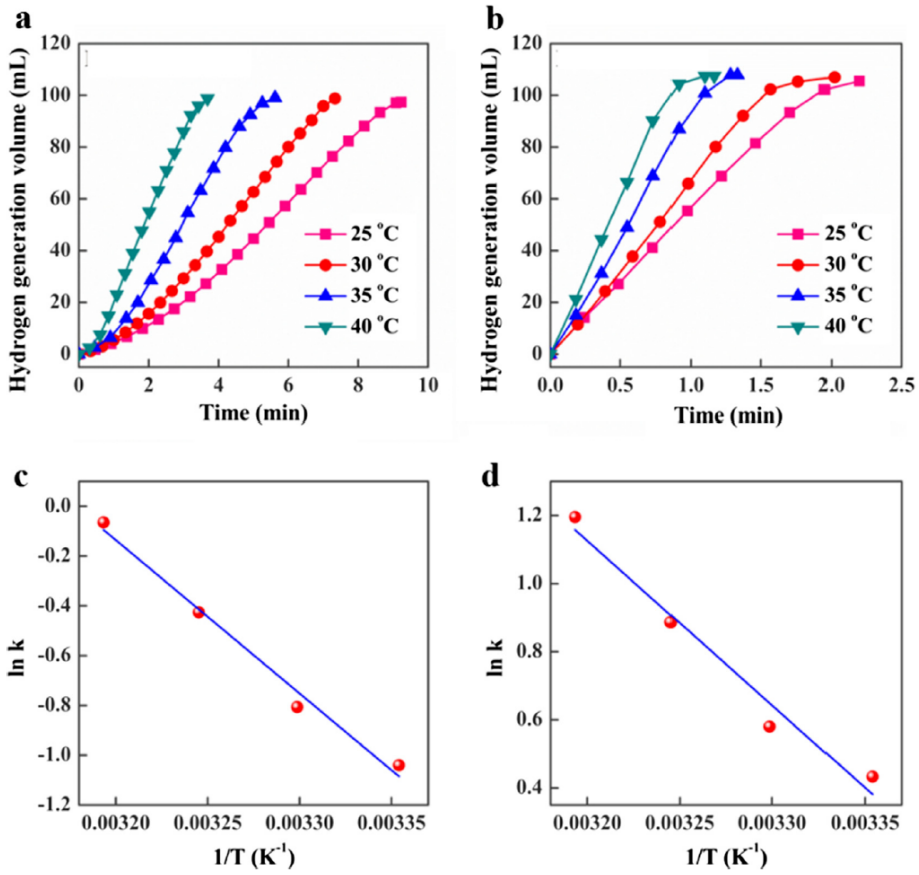

Fig. 2. Hydrogen generation volume as a function of time over Pt/CNT-in situ (a) and Pt/CNT-ex situ (b) catalysts at 25, 30, 35 and 40 °C. Corresponding ln k as a function of 1/T for Pt/CNT-in situ (c) and Pt/CNT-ex situ (d) catalysts. Reaction conditions: V_{AB} = 5 mL, c_{AB} = 0.32 mol/L.

Pt nanoparticles supported on CNT were generated in situ from the reduction of Pt precursors during the catalytic hydrolysis of AB, where the resultant catalyst was labeled as Pt/CNT-in situ. In a typical experiment, the as-synthesized catalyst precursor was preloaded into a three-necked flask, and a water bath was used to control the temperature of the reaction solution. The reaction was started by rapid injection of an aqueous AB solution (5 mL and 0.01 g mL^{-1}) into the flask via a syringe. The AB solution was mixed well with the precursor using a magnetic stirrer, and the molar ratio of Pt to AB (i.e., n_{Pt}/n_{AB}) was 0.0047. The flask was connected to a water-filled gas burette, and an electronic balance was used to measure the volume of the discharged water. The volume of discharged water could be further converted into the volume of generated hydrogen. After the completed release of hydrogen, the used catalyst was isolated from the spent reaction solution for further characterization.

For comparison, another Pt/CNT catalyst was prepared by ex situ reduction with H_2 at 250 °C for 2 h and labeled as Pt/CNT-ex situ for the reaction. Based on our previous work, the Pt loading was held at 6.0 wt% to obtain Pt nanoparticles over the Pt/CNT-ex situ catalyst that were similarly sized compared with the Pt/CNT-in situ catalyst and thus nearly exclude the Pt size effects (Chen et al., 2014a). The reduced Pt/CNT-ex situ catalyst was cooled to room temperature under Ar atmosphere, passivated by 1.0 vol% O_2/Ar for 20 min, and held under an inert atmosphere before testing and characterization.

For the above two Pt/CNT catalysts, isotopic experiments using D_2O instead of H_2O as the reactant were conducted to explore the effects of Pt surface and electronic properties on the ability to activate water. Additionally, durability testing was performed to explore these surface and electronic property effects on the catalyst durability. For durability testing, an additional 5 mL AB solution was added to the reactor after the completion of the last run. A similar operation was repeated four times. After the sixth run, the deactivated catalyst was isolated from the spent reaction solution for further characterization.

2.2. Characterization

The size distribution and mean particle size of the Pt nanoparticles on the catalysts were determined by measuring more than 200 individual nanoparticles with high-angle annular dark-field scanning transmission electron microscopy (HAADF-STEM) images obtained on a Tecnai G2 F20 S-Twin equipped with a digitally processed STEM imaging system. High-resolution transmission electron microscopy (HRTEM) observations of Pt nanoparticles were performed with a JEOL JSM-2100 electron microscope. ICP atomic emission spectrometry (Agilent 725-ES ICP AES) was applied to analyze the elemental contents. X-ray photoelectron spectrometry (XPS) was performed on a Kratos XSAM 800 spectrometer (Manchester, UK) equipped with an Al K_α X-ray (1486.6 eV, excitation source at 15 kV). The samples were held under an inert atmosphere at room temperature prior to XPS measurement, and the binding energies were calibrated based on the graphite C 1s peak at 284.6 eV. FTIR spectra were recorded using a Perkin Elmer Spectrum 100 FTIR spectrometer. Raman measurements were collected using a LabRam HR-UV (HORIBA Jobin Yvon).

3. Results and discussion

3.1. Kinetic and isotopic analyses

To nearly exclude the Pt size effects, two Pt/CNT catalysts with similar Pt particle sizes (Fig. 1a and b) were tested for the reaction, and Fig. 1c and d show that they exhibit significantly different catalytic behaviors. In principle, Pt^{n+} ions supported on CNT can be reduced by AB during hydrolysis. With the addition of AB solution into the suspension of Pt/CNT precursors, both reduction of Pt^{n+} to Pt^0 and H_2 generation from hydrolytic dehydrogenation of AB occur simultaneously. The progress of the Pt^{n+} reduction and concomitant hydrolytic dehydrogenation of ammonia borane was followed by monitoring the H_2 generation volume. Interestingly, the Pt/CNT-in situ catalyst presents three kinetic regimes: (I) a gradual increase in the hydrogen generation rate with reaction time in the initial period, likely arising from the gradual in situ reduction of the Pt/CNT catalyst precursor with AB; (II) a linear increase in hydrogen generation volume with time in the range of 2–6 min; and (III) a regime with decreasing rates.

In contrast, the Pt/CNT-ex situ catalyst reveals a nearly linear increase in the hydrogen volume except at the latest stage of the reaction. The linearly increased hydrogen volumes with reaction time suggest a zero-order reaction with respect to AB, and therefore, their slopes can be used to determine the reaction rates (Chen et al., 2014a). The resultant reaction rates can be further correlated with particle size to evaluate the influence of Pt NPs size. It can be clearly observed in Fig. 1e that the Pt/CNT-ex situ catalyst delivers much higher catalytic activity than the Pt/CNT-in situ catalyst and a nearly four times higher reaction rate at a similar size within the standard deviation. Thus the particle size can be excluded as a main driver of the large difference in catalytic activity for these two catalysts.

Kinetic and isotopic analyses were further conducted to gain insight into the significantly different catalytic behaviors. It can be clearly observed in Figs. 1f and 2 that the Pt/CNT-in situ catalyst exhibits higher activation energy than the Pt/CNT-ex situ catalyst,

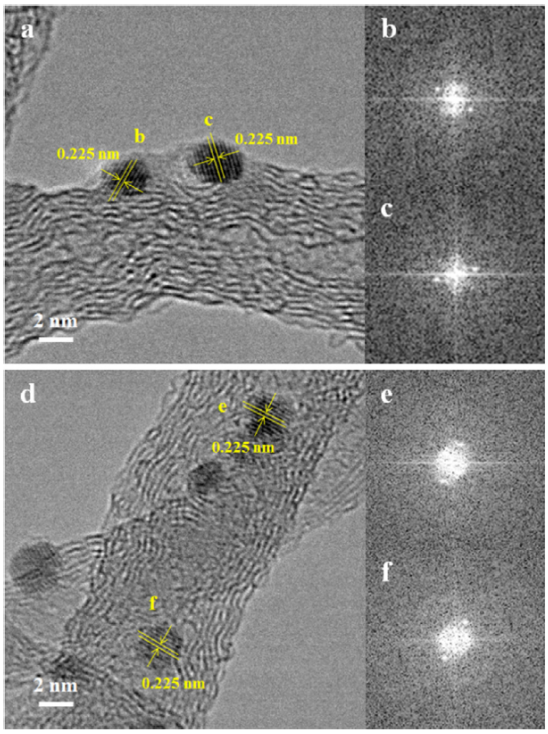

Fig. 3. Representative HRTEM images and their corresponding FFT patterns for Pt/CNT-in situ (a–c) and Pt/CNT-ex situ (d–f) catalysts.

which provides an interpretation for the former catalyst with the lower hydrogen generation activity mentioned previously. Additionally, as shown in Fig. 1c and d, isotopic experiments using D_2O instead of H_2O as a reactant showed that both catalysts exhibit much slower reaction rates. Based on the ratio of the rate constants between H_2O and D_2O as the reactants, i.e., k_H/k_D, their kinetic isotope effect (KIE) values were determined to be 4.94 and 2.75, respectively. These large and different KIE values indicate the O—H bond cleavage of H_2O as the rate-determining step and explain the two catalysts with different abilities to activate water. According to previous studies (Chen et al., 2000; Koshino et al., 2003), the smaller KIE value for the Pt/CNT-ex situ catalyst suggests favorable activation of water. It is worth noting that for the two similarly sized Pt/CNT catalysts, the difference in the KIE values arises in principle from the different surface and/or electronic properties of the two catalysts.

3.2. Characterization of surface and electronic properties

Furthermore, multiple techniques were applied to explore the differences in the surface and electronic properties of the two catalysts. HRTEM measurements were first conducted, and the representative images are shown in Fig. 3a and d. Both catalysts show certain typical Pt nanoparticles with an inter-planar spacing of 0.225 nm, which corresponds to the (111) lattice spacing of face-centered cubic Pt. This observation is confirmed by the corresponding FFT patterns (Fig. 3b, c, e and f). Notably, two unexpected phenomenon occur: (i) a legible crystalline form of Pt nanoparticles on the Pt/CNT-in situ catalyst, which could be due to a reduction mechanism of the Pt catalyst precursor with AB that differs from that of the non-noble catalyst precursor with AB (leading to the formation of amorphous non-noble nanoparticles upon the AB reduction), and (ii) in situ reduction with AB as an ineffective method for synthesis of a highly active noble Pt catalyst because the resultant Pt/CNT catalyst from the in situ reduction with AB shows much lower hydrogen generation activity than the Pt/CNT-ex situ catalyst (Fig. 1c and d).

As the reaction proceeds, the resultant B-containing species byproduct adsorb on the catalyst surfaces, which can affect the catalyst electronic properties. To this end, ICP-AES analyses of the used two catalysts were performed after the first run to probe the difference in the adsorption of B-containing species on the

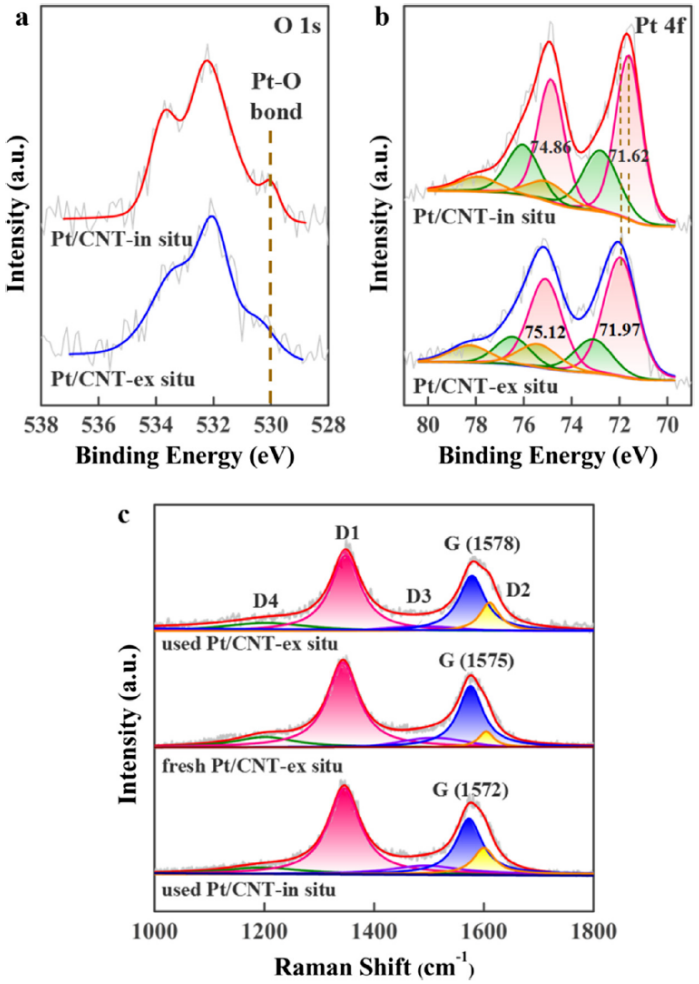

Fig. 4. XPS spectra of O 1s (a) and Pt 4f (b) over Pt/CNT-in situ and Pt/CNT-ex situ catalysts. (c) Raman spectra of fresh and used Pt/CNT-ex situ catalysts and used Pt/CNT-in situ catalyst.

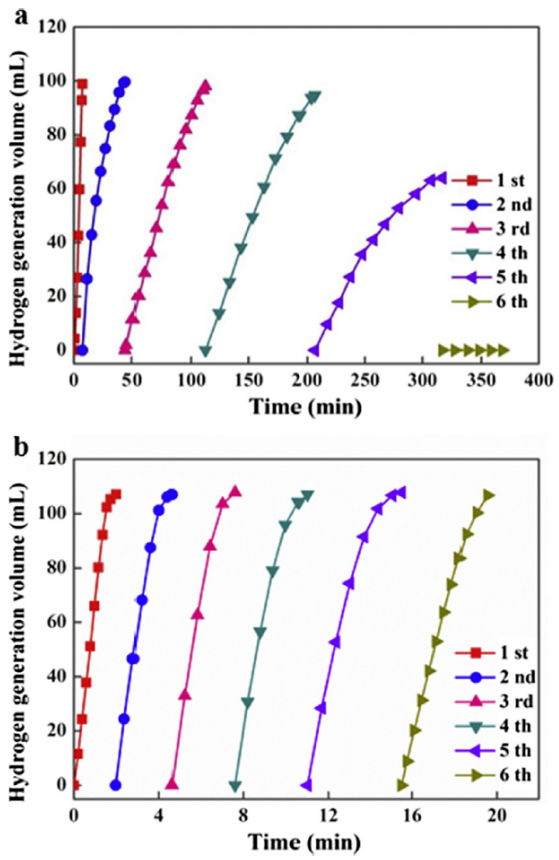

Fig. 5. Durability results of Pt/CNT-in situ (a) and Pt/CNT-ex situ (b) catalysts. Reaction conditions: T = 30 °C, V_{AB} = 5 mL, c_{AB} = 0.32 mol/L.

two catalysts. It was found that the adsorbed contents of B-containing species are 0.54 and 0.05 wt%, respectively. Considering the two similarly sized Pt/CNT catalysts as well as the same n_{Pt}/n_{AB} ratios and CNT supports applied, the two catalysts have similar surface areas for both Pt nanoparticles. Therefore, the enormous difference in the adsorbed B contents is attributed in principle to the different interactions of catalyst precursors with B-containing species and/or different Pt electronic properties. For the in situ reduction with AB, the Pt species in the catalyst precursors occur in the form of platinum ions, which possibly have a strong interaction with electron negative oxygen in the B-containing species for a higher adsorbed B content. However, the adsorbed B species usually affect the Pt electronic properties (Chen et al., 2014a; Montilla et al., 2004; Park et al., 2011).

To test this idea, FTIR and XPS were used to characterize the surface and electronic properties of the two used catalysts. As shown in the FTIR spectra (Fig. S1), no legible Pt—O and B—O peaks appear, possibly because their characteristic peaks are overlapped with those of the CNT support and the adsorbed B contents are relatively low. Although deconvolution of the O 1s peaks in Fig. 4a was not performed because of a lack of reasonable peak assignments (e.g., B—O bond), the stronger O 1s peak at 530.1 eV over the Pt/CNT-in situ catalyst is most likely assigned to the Pt—O bond arising from the strong interaction of Pt with the O of B-containing species (Borgel et al., 2013; Yue et al., 2015). Moreover, a shoulder appears at 533.6 eV in the Pt/CNT-in situ spectra compared with that of the Pt/CNT-ex situ spectra, which might be due to the interaction of reduction products with the surface oxygen groups on CNT. It can also be observed in Fig. 4b that the deconvolution of the Pt 4f spectra shows lower Pt^0 $4f_{7/2}$ binding energy for the used Pt/CNT-in situ catalyst (i.e., 71.62 eV) than the used Pt/CNT-ex situ catalyst (i.e., 71.97 eV). The higher Pt^0 $4f_{7/2}$ binding energy can explain why the Pt/CNT-ex situ catalyst exhibits much higher hydrogen generation activity.

Selected previous studies demonstrated that the adsorption of B-containing species on the catalyst surfaces leads to the strong interaction of Pt with B of the B-containing species and thus an increase in the metal binding energies through electron transfer from the metal to electron-deficient B (Montilla et al., 2004; Park et al., 2011). However, for the two similarly sized Pt nanoparticles supported on CNT catalysts and the same molar Pt used in the reaction, the used Pt/CNT-in situ catalyst shows a lower Pt^0 $4f_{7/2}$ binding energy than the fresh Pt/CNT-ex situ catalyst (Fig. S2), whereas the used Pt/CNT-ex situ catalyst displays higher Pt^0 $4f_{7/2}$ binding energy instead. This observation indicates that the in situ reduction with AB leads to a different interaction between the Pt and B-containing species over the Pt/CNT-in situ catalyst against the Pt/CNT-ex situ catalyst, i.e., Pt—O bonding versus the interaction of Pt with B.

To obtain additional details into the electron transfer of the two catalysts, Raman measurements were further conducted because

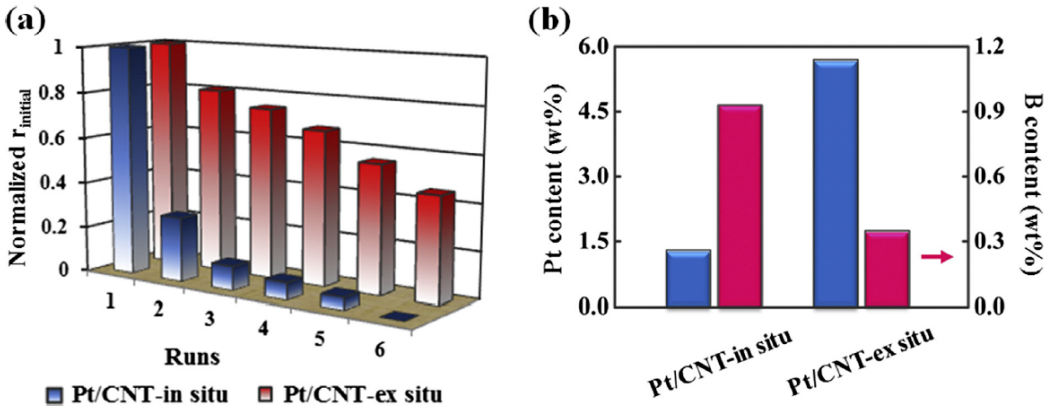

Fig. 6. Relative activities over runs (a) and adsorbed B contents (b) of deactivated Pt/CNT in-situ and Pt/CNT-ex situ catalysts.

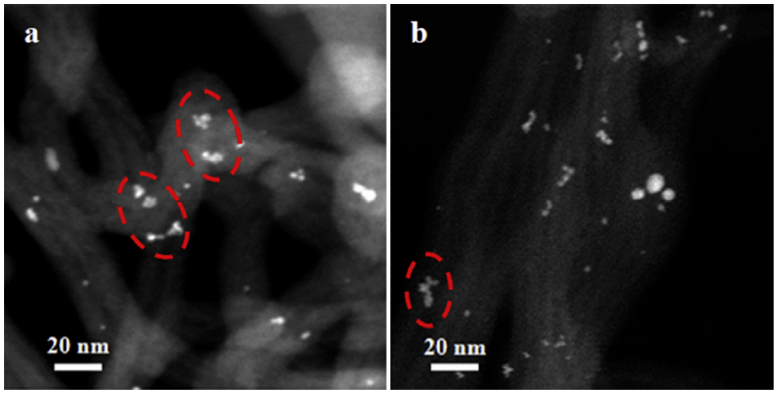

Fig. 7. Typical HAADF-STEM images of deactivated Pt/CNT-in situ (a) and Pt/CNT-ex situ (b) catalysts.

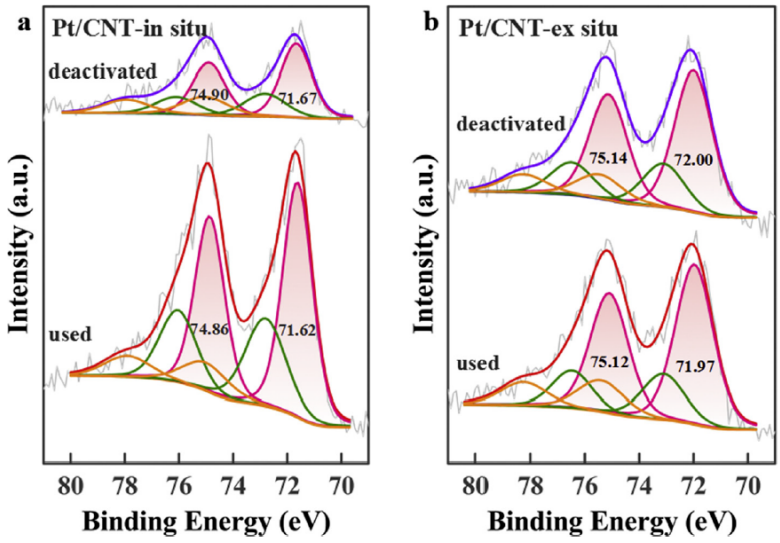

Fig. 8. Typical XPS Pt 4f spectra of used and deactivated Pt/CNT-in situ (a) and Pt/CNT-ex situ (b) catalysts.

Raman scattering is strongly sensitive to the electronic properties of carbon-based catalysts, and G-band shifts have been suggested due to the electron transfer between the metal and support (Sgobba and Guldi, 2009; Dennany et al., 2010). As shown in Fig. 4c, compared with the fresh Pt/CNT-ex situ catalyst, the used Pt/CNT-in situ catalyst exhibits a downshift of 3 cm^{-1} in the G-band, whereas the used Pt/CNT-ex situ catalyst shows an upshift of 3 cm^{-1}. This information is consistent with the XPS results shown in Fig. 4 and S2. Fig. 4c obviously reveals that both the used Pt/CNT-in situ and Pt/CNT-ex situ catalysts show values of I_{D2}/I_G that are approximately two times larger than that of the fresh Pt/CNT-ex situ catalyst. This observation might suggest similar adsorbed contents of B-containing species on the support (Sadezky et al., 2005). Therefore, it could be deduced again that the different electronic properties of the two catalysts can strongly contribute to the different interactions of Pt with B-containing species. All of the above results demonstrate the crucial impacts of the catalyst reduction method on the surface and electronic properties of the catalysts and thus the hydrogen generation activity.

In addition to the crucial impacts of the surface and electronic properties of the two catalysts, their impacts on durability were also systematically explored. To this end, the new AB solution was added into the reactor after completion of the last run, and similar operations were repeated another four times. As shown in Fig. 5, both catalysts show gradually decreased hydrogen generation activities with run number. To make a clear and direct comparison of the durability between the two catalysts, the deactivation function was defined as the reaction rate in each run normalized by that of the first run. Fig. 6a presents the relative activities over the run number of the two catalysts. Obviously, the Pt/CNT-ex situ catalyst has much higher durability than the Pt/CNT-in situ catalyst. Especially for the resultant Pt/CNT catalyst from the in situ reduction with AB, a dramatic decrease was observed in the reaction rate at the 2nd run, i.e., only ~28% activity was retained. This result could be ascribed to the dramatic loss of Pt active sites by the formation of more Pt—O bonds on the Pt/CNT-in situ catalyst and the lower Pt 4f binding energy in terms of more B-containing species adsorption on the catalyst surface

(shown in Fig. 4). More significantly, the hydrogen generation for the Pt/CNT-in situ catalyst ceased at the 6th run.

To understand the remarkably different durability of the two catalysts, ICP-AES was first used to detect the compositions of the filtrates. No detectable platinum species were found in the filtrate. Furthermore, multiple techniques were used to characterize the difference in the surface and electronic properties of the two deactivated catalysts isolated from the 6th spent reaction solution. The HAADF-STEM measurements in Fig. 7 show that both deactivated catalysts contain a certain amount of agglomerations with irregular shapes compared with the two used catalysts (Fig. 1a and b), but most Pt nanoparticles are still in the range of 2–5 nm. This observation cannot explain why the used Pt/CNT-in situ catalyst from the 5th run is nearly inactive for the reaction in Fig. 5a and 6a. Therefore, it could be deduced that the difference in the surface adsorbed B-containing species and the electronic properties of the two catalysts lead to distinctly different catalyst durabilities.

Furthermore, ICP-AES was used to determine the contents of Pt and the adsorbed B-containing species on the two deactivated catalysts. As shown in Fig. 6b, the Pt contents actually loaded on CNT measured by ICP-AES were 1.3 and 5.6 wt% for the deactivated Pt/CNT-in situ and Pt/CNT-ex situ catalysts, respectively. Compared with the theoretical Pt loading of 1.5 and 6.0 wt% for the two catalysts, this evidence suggests that the in situ reduction with AB has less influence on the leaching of Pt over CNT and that the metal loss during the reaction is negligible. Moreover, the adsorbed B contents are determined to be 0.93 and 0.35 wt%, respectively. In fact, these adsorbed B-containing species are located not only at the Pt nanoparticle surfaces but also on the support surfaces. In particular, the former case significantly changes the number of exposed Pt atoms and the Pt electronic properties. Furthermore, XPS measurements of the used and deactivated catalysts were performed to qualitatively or quantitatively compare the coverage of B-containing species on the Pt surfaces and the Pt electronic properties. It can be observed in Fig. 8 that compared with the two used catalysts after the 1st run, the two deactivated catalysts exhibit slightly higher Pt^0 $4f_{7/2}$ binding energies, which in principle lead to increased hydrogen generation activities according to our previous work (Chen et al., 2014b). This observation indicates that the change in the Pt electronic properties is not the dominant reason for catalyst deactivation. More interestingly, for the in situ reduction with AB, the deactivated Pt/CNT-in situ catalyst shows a much weaker Pt 4f peak intensity than the used catalyst. Certain previous studies showed that the significantly decreased XPS peak intensity could arise from increased coverage of adsorbates (e.g., B-containing species) (Chen et al., 2015). Therefore, it can be reasonably deduced that the lack of activity of the deactivated Pt/CNT-in situ catalyst after the 5th run could arise from the nearly complete encapsulation of Pt surfaces by the accumulated B-containing species.

3.3. Nature of Pt in contact with AB

Based on the above systematic analyses, the catalyst reduction method has crucial impacts on the surface and electronic properties of the resultant Pt nanoparticles supported on CNT and thus the hydrogen generation activity and durability, as schematically shown in Scheme 1. For the two similarly sized Pt nanoparticles supported on CNT catalysts and the same n_{Pt}/n_{AB} ratios used in this work, during the in situ reduction process with AB, the strong interaction of the Pt species over the Pt/CNT catalyst precursors with the electron-negative oxygen in the B-containing species leads to the formation of Pt—O bonds and thus a decrease in the Pt^0 4f binding energy. However, for the ex situ reduction with H_2, the resultant Pt/CNT-ex situ catalyst exhibits higher Pt^0 4f binding energy with the less negative interference of the Pt—O bonds. This remarkable difference in the surface and electronic properties of the two catalysts can lead to different catalytic behaviors. In addition, the Pt/CNT-in situ catalyst contains more

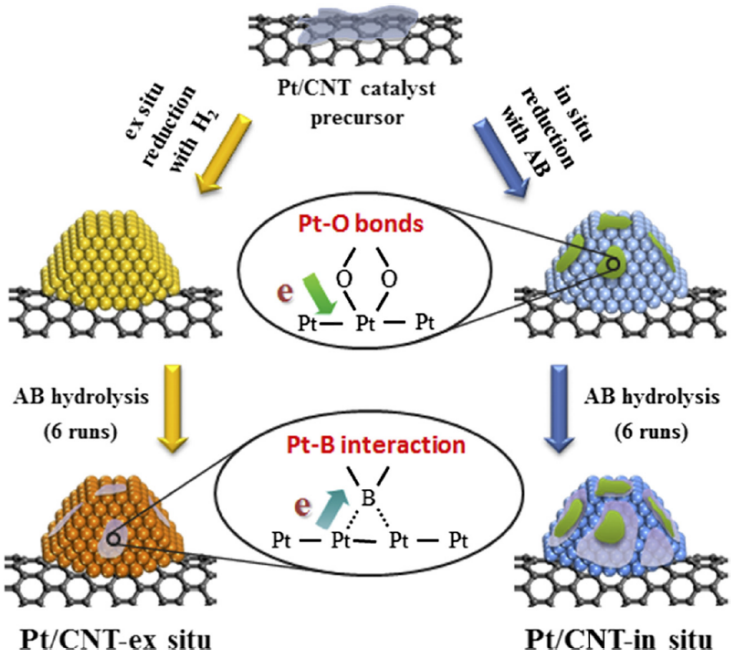

Scheme 1. Schematic diagram of the impacts of catalyst reduction methods on the surface and electronic properties of Pt/CNT catalyst for hydrogen generation from AB.

numerous Pt—O bonds on the catalyst surface, and its lower Pt^0 4f binding energy facilitates the adsorption of B-containing species due to the strong interaction of Pt with B, which results in the dramatic loss of Pt active sites. After the 5th run, the Pt nanoparticles are almost completely encapsulated by the B-containing species and thus nearly inactive for the reaction.

4. Conclusions

In summary, by combining kinetic and isotopic analyses with multiple techniques such as HRTEM, HAADF-STEM, XPS, Raman and ICP-AES, we have addressed certain unresolved details of the highly significant impacts of the catalyst reduction methods (i.e., the in situ reduction with AB and the ex situ reduction with H_2) on the hydrogen generation activity and durability. Compared with the Pt/CNT-in situ catalyst, the Pt/CNT-ex situ catalyst exhibits a unique surface (e.g., fewer Pt—O bonds) and electronic properties (e.g., higher Pt binding energy), which give rise to lower activation energy and a stronger ability to activate water and thus produce the higher activity. The differences in the number of the Pt—O bonds and the adsorption or even encapsulation of Pt nanoparticles by the B-containing species are primarily responsible for the different catalyst durability of the two catalysts. The methodology revealed in this work offers insights into the catalyst prepara tion-structure-performance relationship, which might be applied to better understand the relationships of other catalysts in general.

Declaration of competing interests

The authors declare no competing financial interests.

Acknowledgments

This work was financially supported by the Natural Science Foundation of China (21306046), the Shanghai Natural Science Foundation (17ZR1407300 and 17ZR1407500), the Shanghai Rising-Star Program (17QA1401200), Fundamental Research Funds for the Central Universities (222201718003 and WA1514013), the Open Project of State Key Laboratory of Chemical Engineering (SKL-Che-15C03), and the 111 Project of the Ministry of Education of China (B08021).

Appendix A. Supplementary material

Supplementary data associated with this article can be found, in the online version, at http://dx.doi.org/10.1016/j.ces.2017.05.056.

References

Akbayrak, S., Tonbul, Y., Ozkar, S., 2016. Ceria supported rhodium nanoparticles: superb catalytic activity in hydrogen generation from the hydrolysis of ammonia borane. Appl. Catal. B: Environ. 198, 162–170.

Borgel, V., Gershinsky, G., Hu, T., Theivanayagam, M.G., Aurbach, D., 2013. $LiMn_{0.8}Fe_{0.2}PO_4/Li_4Ti_5O_{12}$, a possible Li-ion battery system for load-leveling application. J. Electrochem. Soc. 160, 650–657.

Cao, N., Luo, W., Cheng, G.Z., 2013. One-step synthesis of graphene supported Ru nanoparticles as efficient catalysts for hydrolytic dehydrogenation of ammonia borane. Int. J. Hydrogen Energy 38, 11964–11972.

Chandra, M., Xu, Q., 2006a. Dissociation and hydrolysis of ammonia-borane with solid acids and carbon dioxide: an efficient hydrogen generation system. J. Power Sources 159, 855–860.

Chandra, M., Xu, Q., 2007. Room temperature hydrogen generation from aqueous ammonia-borane using noble metal nano-clusters as highly active catalysts. J. Power Sources 168, 135–142.

Chen, K., Iglesia, E., Bell, A.T., 2000. Kinetic isotopic effects in oxidative dehydrogenation of propane on vanadium oxide catalysts. J. Catal. 192, 197–203.

Chen, W.Y., Ji, J., Feng, X., Duan, X.Z., Qian, G., Li, P., Zhou, X.G., Chen, D., Yuan, W.K., 2014a. Mechanistic insight into size-dependent activity and durability in Pt/CNT catalyzed hydrolytic dehydrogenation of ammonia borane. J. Am. Chem. Soc. 136, 16736–16739.

Chen, W.Y., Ji, J., Duan, X.Z., Qian, G., Li, P., Zhou, X.G., Chen, D., Yuan, W.K., 2014b. Unique reactivity in Pt/CNT catalyzed hydrolytic dehydrogenation of ammonia borane. Chem. Commun. 50, 2142–2144.

Chen, W.Y., Duan, X.Z., Qian, G., Chen, D., Zhou, X.G., 2015. Carbon nanotubes as support in the platinum-catalyzed hydrolytic dehydrogenation of ammonia borane. Chemsuschem 8, 2927–2931.

Chen, W.Y., Li, D.L., Wang, Z.J., Qian, G., Sui, Z.J., Sui, X.Z., Duan, X.Z., Zhou, X.G., Issac, Y., Chen, D., 2017. Reaction mechanism and kinetics for hydrolytic dehydrogenation of ammonia borane on a Pt/CNT catalyst. AIChE J. 63, 60–65.

Cheng, F.Y., Ma, H., Li, Y.M., Chen, J., 2007. $Ni_{1-x}Pt_x$ (x = 0–0.12) hollow spheres as catalysts for hydrogen generation from ammonia borane. Inorg. Chem. 46, 788–794.

Demirci, U.B., Miele, P., 2009. Sodium borohydride versus ammonia borane, in hydrogen storage and direct fuel cell applications. Energy Environ. Sci. 2, 627–637.

Dennany, L., Sherrell, P., Chen, J., Innis, P.C., Wallace, G.G., Minett, A.I., 2010. EPR characterisation of platinum nanoparticle functionalised carbon nanotube hybrid materials. Phys. Chem. Chem. Phys. 12, 4135–4141.

Dillon, A.C., Jones, K.M., Bekkedahl, T.A., Kiang, C.H., Bethune, D.S., Heben, M.J., 1997. Storage of hydrogen in single-walled carbon nanotubes. Nature 386, 377–379.

Koshino, N., Cai, Y., Espenson, J.H., 2003. Kinetic study of the phthalimide N-Oxyl (PINO) radical in acetic acid. Hydrogen abstraction from C—H bonds and evaluation of O—H bond dissociation energy of N-hydroxyphthalimide. J. Phys. Chem. A 107, 4262–4267.

Marder, T.B., 2007. Der Ammoniak-Boran-Komplex: ein Automobiltreibstoff der Zukunft? Angew. Chem. 119, 8262–8264.

Metin, O., Sahin, S., Ozkar, S., 2009. Water-soluble poly(4-styrenesulfonic acid-co-maleic acid) stabilized ruthenium(0) and palladium(0) nanoclusters as highly active catalysts in hydrogen generation from the hydrolysis of ammonia-borane. Int. J. Hydrogen Energy 34, 6304–6313.

Metin, O., Mazumder, V., Ozkar, S., Sun, S., 2010. Monodisperse nickel nanoparticles and their catalysis in hydrolytic dehydrogenation of ammonia borane. J. Am. Chem. Soc. 132, 1468–1469.

Montilla, F., Morallon, E., De Battisti, A., Barison, S., Daolio, S., Vasquez, J.L., 2004. Preparation and characterization of antimony-doped tin dioxide electrodes. 3. XPS and SIMS characterization. J. Phys. Chem. B 108, 15976–15981.

Mori, K., Miyawaki, K., Yamashita, H., 2016. Ru and Ru-Ni nanoparticles on TiO_2 support as extremely active catalysts for hydrogen production from ammonia-borane. ACS Catal. 6, 3128–3135.

Park, H., Kim, Y.K., Choi, W., 2011. Reversing CdS preparation order and its effects on photocatalytic hydrogen production of CdS/Pt-TiO_2 hybrids under visible light. J. Phys. Chem. C 115, 6141–6148.

Peng, B., Chen, J., 2008. Ammonia borane as an efficient and lightweight hydrogen storage medium. Energy Environ. Sci. 1, 479–483.

Rosi, N.L., Eckert, J., Eddaoudi, M., Vodak, D.T., Kim, J., Okeeffe, M., Yaghi, O.M., 2003. Hydrogen storage in microporous metal-organic frameworks. Science 300, 1127–1129.

Sadezky, A., Muckenhuber, H., Grothe, H., Niessner, R., Poschl, U., 2005. Raman microspectroscopy of soot and related carbonaceous materials: spectral analysis and structural information. Carbon 43, 1731–1742.

Sahiner, N., Butun, S., Turhan, T., 2012. P(AAGA) hydrogel reactor for in situ Co and Ni nanoparticle preparation and use in hydrogen generation from the hydrolysis of sodium borohydride. Chem. Eng. Sci. 82, 114–120.

Sanyal, U., Demirci, U.B., Jagirdar, B.R., Miele, P., 2011. Hydrolysis of ammonia borane as a hydrogen source: fundamental issues and potential solutions towards implementation. Chemsuschem 4, 1731–1739.

Schlapbach, L., Zuttel, A., 2011. Hydrogen-storage materials for mobile applications. Nature 414, 353–358.

Sgobba, V., Guldi, D.M., 2009. Carbon nanotubes-electronic/electrochemical properties and application for nanoelectronics and photonics. Chem. Soc. Rev. 38, 165–184.

Staubitz, A., Robertson, A.P.M., Manners, I., 2010. Ammonia-borane and related compounds as dihydrogen sources. Chem. Rev. 110, 4079–4124.

Tang, Z.W., Chen, H., Chen, X.W., Wu, L.M., Yu, X.B., 2012. Graphene oxide based recyclable dehydrogenation of ammonia borane within a hybrid nanostructure. J. Am. Chem. Soc. 134, 5464–5467.

Wang, X., Liu, D.P., Song, S.Y., Zhang, H.J., 2012. Synthesis of highly active Pt-CeO_2 hybrids with tunable secondary nanostructures for the catalytic hydrolysis of ammonia borane. Chem. Commun. 48, 10207–10209.

Wang, X., Liu, D.P., Song, S.Y., Zhang, H.J., 2013. Graphene oxide induced formation of Pt-CeO_2 hybrid nanoflowers with tunable CeO_2 thickness for catalytic hydrolysis of ammonia borane. Chem. Eur. J. 19, 8082–8086.

Wang, S., Zhang, D., Ma, Y.Y., Zhang, H., Gao, J., Nie, Y.T., Sun, X.H., 2014. Aqueous solution synthesis of Pt-M (M = Fe Co, Ni) bimetallic nanoparticles and their catalysis for the hydrolytic dehydrogenation of ammonia borane. ACS Appl. Mater. Interfaces 6, 12429–12435.

Xu, Q., Chandra, M., 2006b. Catalytic activities of non-noble metals for hydrogen generation from aqueous ammonia-borane at room temperature. J. Power Sources 163, 364–370.

Yadav, M., Xu, Q., 2012. Liquid-phase chemical hydrogen storage materials. Energy Environ. Sci. 5, 9698–9725.

Yan, J.M., Zhang, X.B., Han, S., Shioyama, H., Xu, Q., 2008. Iron-nanoparticle-catalyzed hydrolytic dehydrogenation of ammonia borane for chemical hydrogen storage. Angew. Chem. Int. Ed. 47, 2287–2289.

Yan, J.M., Zhang, X.B., Han, S., Shioyama, H., Xu, Q., 2009. Synthesis of longtime water/air-stable Ni nanoparticles and their high catalytic activity for hydrolysis of ammonia-borane for hydrogen generation. Inorg. Chem. 48, 7389–7393.

Yan, J.M., Zhang, X.B., Shioyama, H., Xu, Q., 2010. Room temperature hydrolytic dehydrogenation of ammonia borane catalyzed by Co nanoparticles. J. Power Sources 195, 1091–1094.

Yang, Y.W., Lu, Z.H., Hu, Y.J., Zhang, Z.J., Shi, W.M., Chen, X.S., Wang, T.T., 2014. Facile in situ synthesis of copper nanoparticles supported on reduced graphene oxide for hydrolytic dehydrogenation of ammonia borane. RSC Adv. 4, 13749–13752.

Yao, Q.L., Shi, W.M., Feng, G., Lu, Z.H., Zhang, X.L., Tao, D.J., Kong, D.J., Chen, X.S., 2014. Ultrafine Ru nanoparticles embedded in SiO_2 nanospheres: highly efficient. J Power Sources 257, 293–299.

Yue, H.Y., Wang, Q.X., Shi, Z.P., Ma, C., Ding, Y.M., Huo, N.N., Zhang, J., Yang, S.T., 2015. Porous hierarchical nitrogen-doped carbon coated $ZnFe_2O_4$ composites as high performance anode materials for lithium ion batteries. Electrochim. Acta 180, 622–628.

Zhang, X.B., Yan, J.M., Han, S., Shioyama, H., Xu, Q., 2009. Magnetically recyclable Fe@Pt core-shell nanoparticles and their use as electrocatalysts for ammonia borane oxidation: the role of crystallinity of the core. J. Am. Chem. Soc. 131, 2778–2779.